Molecular dynamics in perfluoroneicosane. II. Components of disorder

Thomas Albrecht, Helmut Elben, Raimund Jaeger, Martin Kimmig, Ralf Steiner, Gert Strobl, Bernd Stühn, Heinz Schwickert, and Clemens Ritter

Citation: The Journal of Chemical Physics **95**, 2807 (1991); doi: 10.1063/1.460932
View online: http://dx.doi.org/10.1063/1.460932
View Table of Contents: http://scitation.aip.org/content/aip/journal/jcp/95/4?ver=pdfcov
Published by the AIP Publishing

Molecular dynamics in perfluoro-*n*-eicosane. II. Components of disorder

Thomas Albrecht, Helmut Elben, Raimund Jaeger, Martin Kimmig, Ralf Steiner, Gert Strobl,[a] and Bernd Stühn
Fakultät für Physik, Universität Freiburg, Hermann-Herder-Strasse 3, 7800 Freiburg, Germany

Heinz Schwickert[b]
Institut für Physikalische Chemie, Universität Mainz, 6500 Mainz, Germany

Clemens Ritter
Institute Laue-Langevin, Grenoble, France

(Received 18 January 1991; accepted 1 May 1991)

The defect structure in the rhombohedral modification *R* of perfluoro-*n*-eicosane has been analyzed in a temperature-dependent x-ray and neutron scattering study. The analysis was based on an evaluation of Bragg-reflection intensities and of the diffuse scattering. Different components of disorder were detected and characterized. At the transition from the low temperature phase to modification *R*, rotation of the molecules about their long axes sets in. As shown by the azimuthal distribution of the diffuse scattering, rotations occur cooperatively with correlations between neighbors. The Debye–Waller factors measured for the layer reflections are indicative for a moderate roughening of the interfaces due to a restricted longitudinal diffusive motion. Molecules are perturbed by the formation of helix reversal defects. Evaluation of the diffuse scattering yields the associated finite azimuthal correlation length. There is also evidence for a continuous slow untwisting of the helix. With increasing temperature, it approaches the all-*trans* form.

INTRODUCTION

At ambient temperature perfluoro-*n*-eicosane ($C_{20}E_{42}$) exhibits the typical properties of a plastic crystal.[1,2] The molecules, which possess a helical conformation, are highly mobile and set up a rhombohedral lattice (modification "*R*"). As described in the first paper of this series,[3] the transition into the plastic phase occurs already at relatively low temperatures, $T_t = 200$ K. In the low temperature phase (modification "*M*", monoclinic lattice, stable at $T < 146$ K), the lattice is built up of arrays of left-handed and right-handed helices in regular order. Between $T = 146$ and 200 K, a third modification occurs. Through all modifications, the positions of the centers of the molecules are retained. The transition to modification *M* is affected by a stop of the motions, and a building up of a superlattice through an ordering of the helices with different handedness. Single crystals in the rhombohedral phase transform into multiple twins, and this occurs without a breaking.

For crystals of oligomeric chain molecules, there exist a number of characteristic motional mechanisms. Longitudinal diffusion, i.e., limited shifts along the chain direction, rotation about the long axis, or mobile intramolecular conformational defects have been observed, mostly in studies on *n*-alkanes (compare Ref. 1, Chap. 10.5). The work presented here deals with the disorder structure in perfluoro-*n*-alkanes. We have determined the mechanisms of motion, which set in at the phase transition, and followed their evolution with increasing temperature.

Investigations on oligomer crystals are not only interesting in their own right, but can also contribute to an understanding of the relaxation behavior of the corresponding polymeric solid, in this case to that of polytetrafluoroethylene (PTFE). In fact, some of the peculiar properties of PTFE, such as toughness and the low surface friction, are certainly associated with a high internal molecular mobility. In PTFE, motion also sets in abruptly, with two phase transitions at 19 and 30 °C.[4] Detailed investigations on polymeric solids are always complicated by their complex partially crystalline morphology. In this situation, studies on oligomer crystals can be helpful by demonstrating possible ways of relaxation.

In order to characterize the defect structure in perfluoro-*n*-eicosane, we have performed x-ray and neutron scattering experiments. Analysis was based on measurements of Bragg intensities and of the diffuse scattering, which is strong in certain regions of reciprocal space and also shows a peculiar structure. It was possible to discriminate between the different components of disorder. We shall deal successively with longitudinal and lateral displacements, helix reversal defects, and correlated chain rotations.

The analysis described in this paper is based on measured static scattering functions. In a continuation, we have also determined dynamic scattering functions at selected wave vectors using quasi- and inelastic neutron scattering. The results of these related dynamical investigations will be reported in next papers of this series.

EXPERIMENTAL

Perfluoro-*n*-eicosane was purchased from SCM/PCR Inc., Gainesville, FL. Neutron scattering experiments were conducted at the Institute Laue-Langevin, Grenoble, France using the powder-diffractometer D1B at wavelengths

[a] To whom correspondence should be addressed.
[b] Present address: Huls AG, 4370 Marl, Germany.

$\lambda = 1.28$ and 2.52 Å. X-ray scattering experiments were partly performed with the help of a powder diffractometer (Siemens D500), partly with a Weissenberg goniometer.

The powder diffractometers require samples with a lateral extension of the order of centimeters. Since we did not succeed in growing single crystals of this size, we used cake samples. "Cakes" were set up of crystals obtained from a solution in trichlorotrifluoroethane. Stacking of the crystals and pressing them together resulted in samples with uniaxial texture, the helix (c) axes being distributed in a range of $\pm 10°$ around the surface normal. Weissenberg exposures were obtained from a single crystal grown from the gas phase by sublimation at $T \approx 360$ K.

SCATTERING PROPERTIES OF DISORDERED CRYSTALS

We begin with a summary of the general scattering properties of disordered crystals.

Disorder in a crystal always leads to a weakening of the Bragg reflections and the appearance of diffuse scattering. These characteristic features are found irrespective of the nature of disorder, which can be either oscillatory or originate from diffusive molecular motions.

As long as the disorder does not destroy the long-range ordered Bravais lattice of the crystal, theoretical treatments of the scattering effects can be based on a consideration of the variations of the unit cell structure factors.[5] Displacements, rotations, or conformational changes of the molecules all result in specific modifications of the structure factor of a given unit cell F_i. The scattering function $S(\mathbf{q})$ of a disordered crystal can be expressed in terms of correlation functions $\langle F_i F_{i+j} \rangle$ associated with these motions. $S(\mathbf{q})$ is generally given by a superposition of Bragg reflections at the reciprocal lattice points S_B and diffuse scattering S_D:

$$S(\mathbf{q}) = S_B(\mathbf{q}) + S_D(\mathbf{q}) \tag{1}$$

with

$$S_B(\mathbf{q}) = |\langle F_i \rangle|^2 \sum \delta(\mathbf{q} - \mathbf{q}_{hkl}) \tag{2}$$

and

$$S_D(\mathbf{q}) = \sum_j \langle (F_i - \langle F_i \rangle)(F^*_{i+j} - \langle F_i \rangle^*) \rangle \exp i\mathbf{q}\cdot\mathbf{x}_j \tag{3}$$

$$= \sum_j \langle \Delta F_i \cdot \Delta F^*_{i+j} \rangle \exp i\mathbf{q}\cdot\mathbf{x}_j \tag{4}$$

($\mathbf{x}_j$ is the lattice vector connecting the unit cells i and $i+j$).

Equation (3) is usually presented in the form

$$S_D(\mathbf{q}) = \langle |\Delta F_i|^2 \rangle \cdot C(\mathbf{q}). \tag{5}$$

The function $C(\mathbf{q})$ introduced by Eq. (5) is associated with the short-range order and defined by

$$C(\mathbf{q}) = \sum_j \frac{\langle \Delta F_i \Delta F^*_{i+j} \rangle}{\langle |F_i|^2 \rangle} \exp i\mathbf{q}_j \cdot \mathbf{x}. \tag{6}$$

In the case of the absence of any short-range order, i.e., of uncorrelated motions of the molecules, $C(\mathbf{q})$ becomes equal to unity.

For the system under study, we now consider the effects of different types of motion, first with regard to the Bragg reflections.

EFFECTS OF DISORDER ON THE BRAGG REFLECTIONS

For a perfect crystal, the structure factors of all unit cells are identical. If we choose for convenience a primitive unit cell [c(prim.) = c(rhomb.)/3, cf. Ref. 3], F_i is directly given by the molecular structure factor F_m. F_m has been given in the previous paper using a series expansion with Bessel functions J_k:

$$F_i = F_m = \sum_{k=-\infty}^{\infty} i^k [f_C J_k(\rho_C q_\rho) + 2 f_F J_k(\rho_F q_\rho) \cos k\beta] \times \exp ik\phi \cdot \sum_{l=0}^{19} \exp i(z_l q_z + k\varphi_l) \tag{7}$$

$$= \sum_{k=-\infty}^{\infty} F^k_m. \tag{8}$$

Here f_C and f_F are the atomic form factors of the carbon and fluorine atoms, ρ_C and ρ_F give their distance from the helix axis, and β is the azimuthal angle difference between a carbon atom and the associated fluorine atoms. The coordinates z_l and φ_l denote the height and the azimuthal angle of the monomer l. F^k_m is the contribution of Bessel functions of order k to F_m. The reciprocal space vector $\mathbf{q}$ is given using cylindrical coordinates (q_ρ, ϕ, q_z).

A displacement u_i of the molecule in cell i along the helix axis means $\delta z_l = u_i$ for all monomers and therefore

$$F_i = \exp iq_z u_i \cdot F_m. \tag{9}$$

If the molecule is rotated about the long axis by an angle $\Delta\varphi_i$, the change of F_i can also be given directly. Replacement of the azimuthal angles φ_l of the monomers by $\varphi_l - \Delta\varphi_i$ results in

$$F_i = \sum_{k=-\infty}^{\infty} \exp -ik\Delta\varphi_i \cdot F^k_m. \tag{10}$$

Translations and rotations lead to different changes of the Bragg intensities

$$S_B(\mathbf{q}_{hkl}) = |\langle F_i \rangle|^2 (\mathbf{q}_{hkl}).$$

Averaging the structure factors for varying translational shifts

$$\langle F_i \rangle = F_m \langle \exp iq_z u_i \rangle \tag{11}$$

and assuming a Gaussian distribution of u_i leads to

$$\langle \exp iq_z u_i \rangle = \exp[-\tfrac{1}{2}\langle (q_z u_i)^2 \rangle] \tag{12}$$

and

$$\langle F_i \rangle = \exp[-\tfrac{1}{2}\langle (q_z u_i)^2 \rangle] \cdot F_m. \tag{13}$$

Taking the average for a distribution of azimuthal turns gives

$$\langle F_i \rangle = \sum_{k=-\infty}^{\infty} \langle \exp -ik\Delta\varphi_i \rangle F^k_m. \tag{14}$$

Assuming also for $\Delta\varphi_i$ a Gaussian distribution, one obtains

$$\langle \exp -ik\Delta\varphi_i \rangle = \exp -\tfrac{1}{2}\langle k^2 \Delta\varphi_i^2 \rangle, \tag{15}$$

which leads to

$$\langle F_i \rangle = \sum_{k=-\infty}^{\infty} \exp(-\tfrac{1}{2}\langle k^2 \Delta\varphi_i^2 \rangle) \cdot F_m^k. \qquad (16)$$

In both cases, longitudinal translation and rotation, the weakening of the mean structure factors and hence of the Bragg reflections is described by generalized Debye–Waller factors. A comparison shows the difference between the effects. Longitudinal translations result in a weakening which depends only on q_z and increases with q_z. Rotations, on the other hand, lead to a weakening which is only a function of q_ρ. It increases with the order k of the Bessel function, which essentially means that the weakening increases with q_ρ (higher order Bessel functions have their first maximum at higher q_ρ's).

Considering these general tendencies, it is possible to give a first characterization of the transition to the rhombohedral phase R. The changes in the scattering pattern at the transition can be summarized as follows (compare Ref. 3):

(i) All reflections which are located away from the equator ($q_z = 0$) and from the meridian are extinguished. In particular, all superlattice reflections disappear.

(ii) There is a moderate weakening of the meridional 001 reflections.

Observation (i) is indicative for a vanishing of all contributions of Bessel functions with $k \neq 0$:

$$\langle F_m^k \rangle = 0 \quad \text{for} |k| > 0.$$

This behavior suggests strongly an onset of chain rotations at the phase transition. Rotations may either correspond to complete turns, which leads to

$$\langle \exp - ik\Delta\varphi_i \rangle = 0,$$

or involve at least a sufficiently large angular range $\langle \Delta\varphi_i^2 \rangle \gg 1$.

Chain rotation also explains the disappearance of the superlattice reflections. Their intensities are generally related to the difference between the structure factors of right- and left-handed helices F_m^r and F_m^l. This difference only results from different contributions by Bessel functions of the order $k \neq 0$; the contributions proportional to J_0 are identical for F_m^l and F_m^r. Hence, superlattice reflections disappear, if chains are rotating, and this even then, when the alternation of right- and left-handed helices found in modification M is retained. There are clear indications for a correlation of the rotations of adjacent molecules. Evidence is given by the shape of the diffuse scattering S_D. Later on we shall come back to this point.

Observation (ii) suggests a slight roughening of the interfaces resulting from small longitudinal diffusive steps. The result of data evaluation is presented in the next chapter.

The transition to modification R therefore resembles a "rotational transition." The onset of chain rotations constitutes the dominant mechanism.

LONGITUDINAL DISORDER

Figure 1 shows the series of meridional reflections (001), as obtained by x-ray scattering at $T = 219$ K using the powder diffractometer D500. Reflection intensities decrease with increasing temperature.

The weakening can be characterized by a Debye–Waller

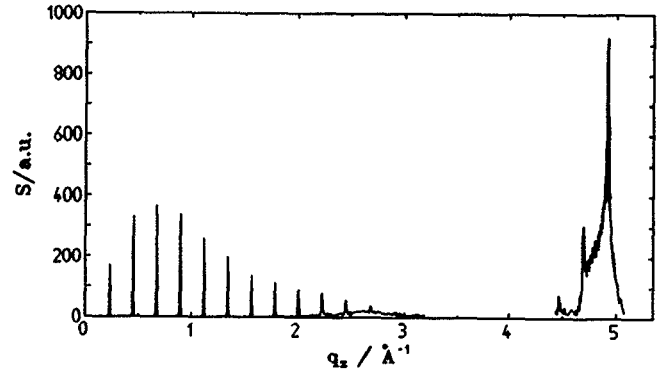

FIG. 1. $C_{20}F_{42}$. X-ray scattering intensity along the meridian, measured for a cake sample with uniaxial texture at $T = 219$ K.

factor, as described by Eq. (13). Determination of the Debye–Waller factors was accomplished as follows: For the cake sample under study, the Lorentz factors $L(\theta)$ related to the orientational order were unknown for the low order reflections $2\theta < 40°$; for the two strong reflections in the range $2\theta = 70°$–$75°$, a dependence $L(\theta) \sim q^{-2}$ could be assumed. In the case of the low order reflections, we first determined Debye–Waller-factor ratios with regard to the values at a reference temperature T_0 (= 237 K). Since

$$I_{ool} \sim \exp - q_l^2 \langle u^2 \rangle \cdot F_m^2(q_l) \cdot L(\theta_l), \qquad (17)$$

one obtains

$$\exp - q_l^2 [\langle u^2 \rangle(T_1) - \langle u^2 \rangle(T_0)] = \frac{I_{ool}(T_1) \cdot F_m^2[q_l(T_0)]}{I_{ool}(T_0) \cdot F_m^2[q_l(T_1)]}, \qquad (18)$$

which is independent of $L(\theta)$. $I_{ool}(T)$ and $q_l(T)$ denote the intensity and the position of the *ool* reflection; both change with temperature.

The evaluation of the higher order reflections on the basis of Eq. (17) with $L \sim q^{-2}$ yielded absolute values $\langle u^2 \rangle(T)$. They were, however, not very precise. Combining both sets of data gave the final result shown in Fig. 2.

The observed mean-squared displacements $\langle u^2 \rangle$ are

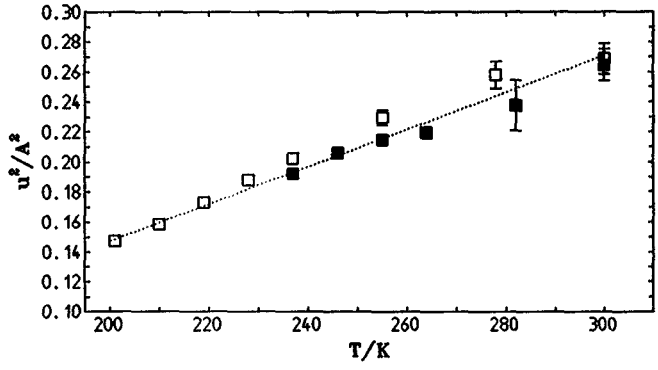

FIG. 2. $C_{20}F_{42}$. Temperature dependence of the mean-squared longitudinal shifts $\langle u_i^2 \rangle$. (□, values derived from high order reflections; ■, adjusted relative values, obtained from low order reflections.)

clearly larger than those usually found in molecular crystals as a consequence of thermal vibrations. The reason for this has been clarified by quasi- and inelastic neutron scattering experiments. As described in detail in paper III of this series, longitudinal motion in phase R is a superposition of oscillations and diffusive longitudinal steps. Regarding the helical form of the molecule, the diffusive steps could be associated with a screw motion rather than being a purely longitudinal mode. Since the helix turn is slow (cf. Figs. 5 and 10), the angular contribution would be only small.

The longitudinal displacements associated with the diffusive steps lead to a roughening of the interfaces. It is interesting to compare this interface perturbation to that found in the high temperature modifications of *n*-alkanes. For *n*-alkanes, the thickness of the perturbed interface region is much larger; it extends over 4–10 Å.[6] We learn from the comparison that chain flexibility, which is given for the *n*-alkanes, is a prerequisite for a pronounced "interface melting." Perfluoro-*n*-alkanes resemble stiff rods and do not allow the necessary tilting of the end groups.

LATERAL DISPLACEMENTS

The lateral displacements of the molecules from their equilibrium positions are also larger than usual. We have analyzed the situation at room temperature. After a determination of the integral intensities I_{h0l} of all visible $h\,0l$ reflections ($|h|\leqslant 4, |l|\leqslant 30$) using a Weissenberg diffractometer, we performed a two-dimensional Fourier synthesis. It yields the mean electron-density distribution in a projection along the b axis onto the xz plane (z running parallel to the c axis; the unit cell is described in Ref. 3)

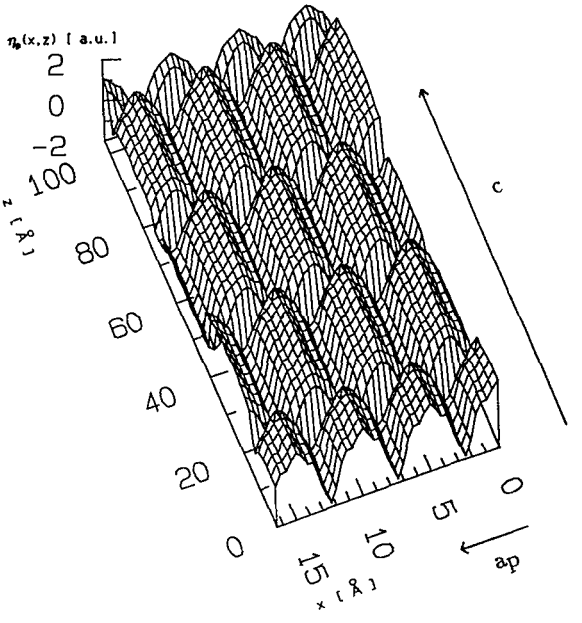

FIG. 3. $C_{20}F_{42}$. $T = 300$ K. Thermal average of the electron density distribution in a projection along the b axis [$\eta_p(x,z)$; a_p denotes the component of the a axis perpendicular to b].

$$\eta_p(x,z) - \sum_{hl} \langle F_{h0l} \rangle \exp i(a^*hx + c^*kz), \tag{19}$$

$$\langle F_{h0l} \rangle \sim \pm I_{h0l}^{1/2}. \tag{20}$$

The sign was taken as that of the perfect lattice, determined by a model calculation.

The result of the Fourier synthesis is given in Fig. 3. The picture shows the projected electron density η_p for a number of stacked layers. The profile corresponds to the thermal average over the motions of the molecules. All structural details of the individual molecules are smeared out. The molecules resemble cylinders. They are displaced from the equilibrium positions in longitudinal and lateral direction, with mean-squared displacements $\langle \Delta z^2 \rangle (= \langle u_l^2 \rangle)$ and $\langle \Delta x^2 \rangle$.

In order to determine $\langle \Delta x^2 \rangle$, we have compared the transverse profile $\eta_p(x, z=0)$ with the results of straightforward model calculations. The atomic electron density distributions were described by Gaussian functions

$$\eta_a(|\mathbf{r}|) = A_a (2\pi\sigma_a^2)^{-3/2} \exp -\frac{r^2}{2\sigma_a^2}, \quad a = \mathrm{F,C}$$

with

$$\sigma_F = 0.275 \text{ Å}, \quad \sigma_C = 0.390 \text{ Å},$$
$$A_F = 9, \qquad A_C = 6.$$

The electron densities contributed by the 42 fluorine and 20 carbon atoms were averaged over cylinders, placing the centers of the fluorine atoms at a distance $\rho_F = 1.63$ Å and those of the carbon atoms at $\rho_C = 0.42$ Å. Finally, lateral displacements of the helix axes were introduced, assuming a Gaussian distribution with a variance $\langle \Delta x^2 \rangle$. Figure 4 shows the results of (a) the model calculation and (b) a fit to the experimental data. An excellent representation of the experimental data is achieved for a mean displacement $\langle \Delta x^2 \rangle^{1/2} = 0.26$ Å.

We associate this comparatively large value with the occurrence of conformational defects. As discussed in the next chapter, helix reversals are introduced into the chains. They may produce a slight bend and therefore result in lateral displacements and an increase in the mean cross section of the molecules. We have also checked for the longitudinal displacements $\langle \Delta z^2 \rangle$. They are in agreement with those derived from the Debye–Waller factors obtained in the x-ray and neutron-scattering experiments described above.

HELIX REVERSAL DEFECTS

The occurrence of "helix reversal defects" has been discussed repeatedly in the literature in works dealing with the defect structure of the high temperature modifications of PTFE.[7–9] First indications were obtained by Brown[7] from IR spectroscopy. A special band was detected, which was assigned to a local mode attached to a conformational defect. Normal mode calculations provided support for a "helix reversal" defect, which is shown in Fig. 5. The defect introduces a change of the helix conformation from a left-handed into a right-handed form. Expressed in terms of rotational angles about the C–C bonds, the defect corresponds to a sequence $\alpha = -15°, -15°, 0°, +15°, +15°$ ($\alpha = 0°$ denotes a trans-conformation).

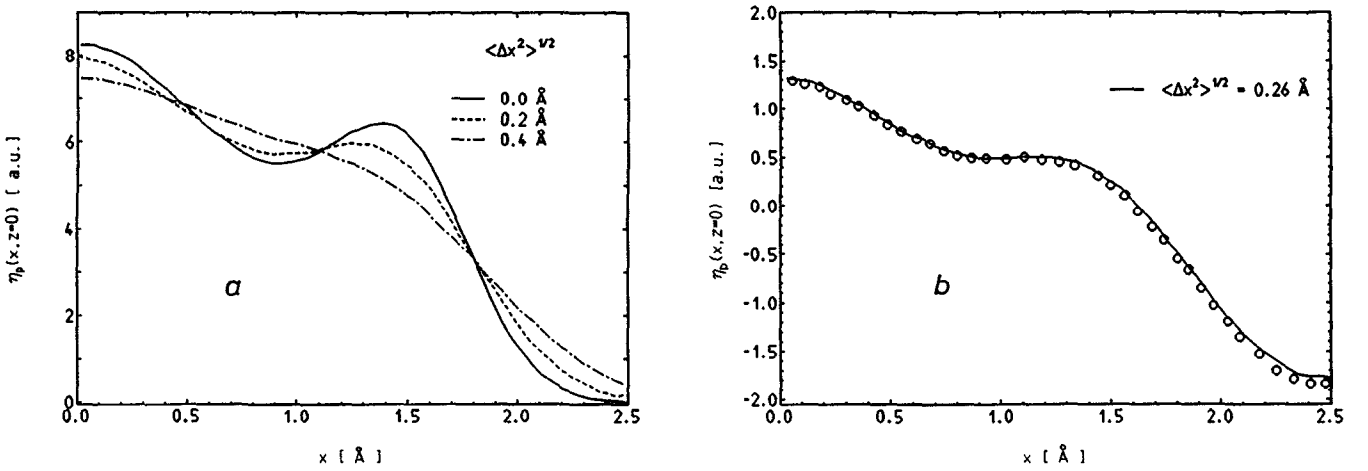

FIG. 4. (a) Transverse electron density profile $\eta_p(x,z=0)$ calculated for a model under variation of the mean-squared lateral displacement $\langle \Delta x^2 \rangle$; (b) fit to the experimental data.

The defect also modifies the structure factor in a characteristic way, as shown by Corradini and Guerra[9] by straightforward calculations. A qualitative agreement with the results of x-ray scattering experiments in the high-temperature phase of PTFE ws obtained.

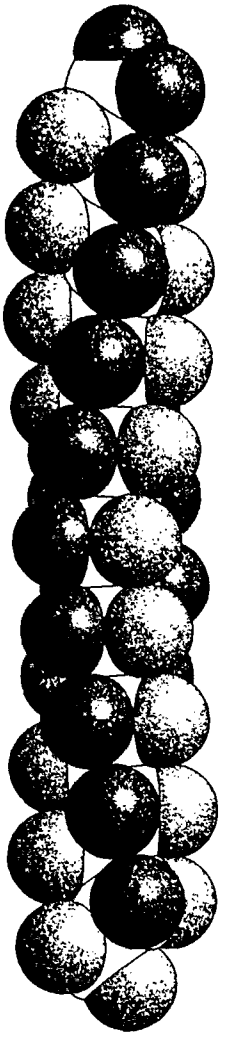

FIG. 5. Helix-reversal defect in a $(CF_2)_n$ chain.

Quite similar observations were made for the system under study. Figure 6 shows the intensity distribution in the range of strong diffuse scattering around $q_\rho = 1.3$ Å^{-1}, $q_z = 2.4$ Å^{-1}, measured at different temperatures above T_t by neutron scattering.

This region is dominated by contributions of the first-order Bessel functions F_m^1. In modification R, the Bragg reflections in this range are completely extinguished by the chain rotation. The diffusive scattering, which shows up instead, presents the molecular structure $\langle |F_m|^2 \rangle$ directly in a thermal average.

As shown in Fig. 6, the intensity distribution changes with increasing temperature in a characteristic way. First, at a temperature just above T_t, two separate maxima show up [Fig. 6(a)]. This intensity distribution corresponds to that expected for unperturbed right-handed or left-handed helices. As described in Ref. 3, analysis enables a direct determination of the helix parameters $\Delta z (= 1.30$ Å) and $u/t (\approx 15/7)$. With increasing temperature, the peaks broaden, approach each other, and finally merge [Fig. 6(d)]. At ambient temperature, only one broad maximum, located in the middle of the previous two, is observed. Figure 7 presents these changes in more detail, giving $S_D(q_z)$ at a constant value of q_ρ.

In order to analyze the data, we have used a general correlation function approach.

Scattering function of a perturbed helix

The diffuse scattering in the range of interest is given by [Eq. (5); $\langle F_i \rangle = 0$]

$$S_D(\mathbf{q}) = \langle |F_i|^2 \rangle \cdot C(\mathbf{q}).$$

Conformational defects in the helix become apparent in the molecular scattering function $\langle |F_i|^2 \rangle$. In the q range under discussion, F_i is dominated by the first order Bessel-function contributions of the fluorine atoms and essentially given by [cf. Eq. (7)]

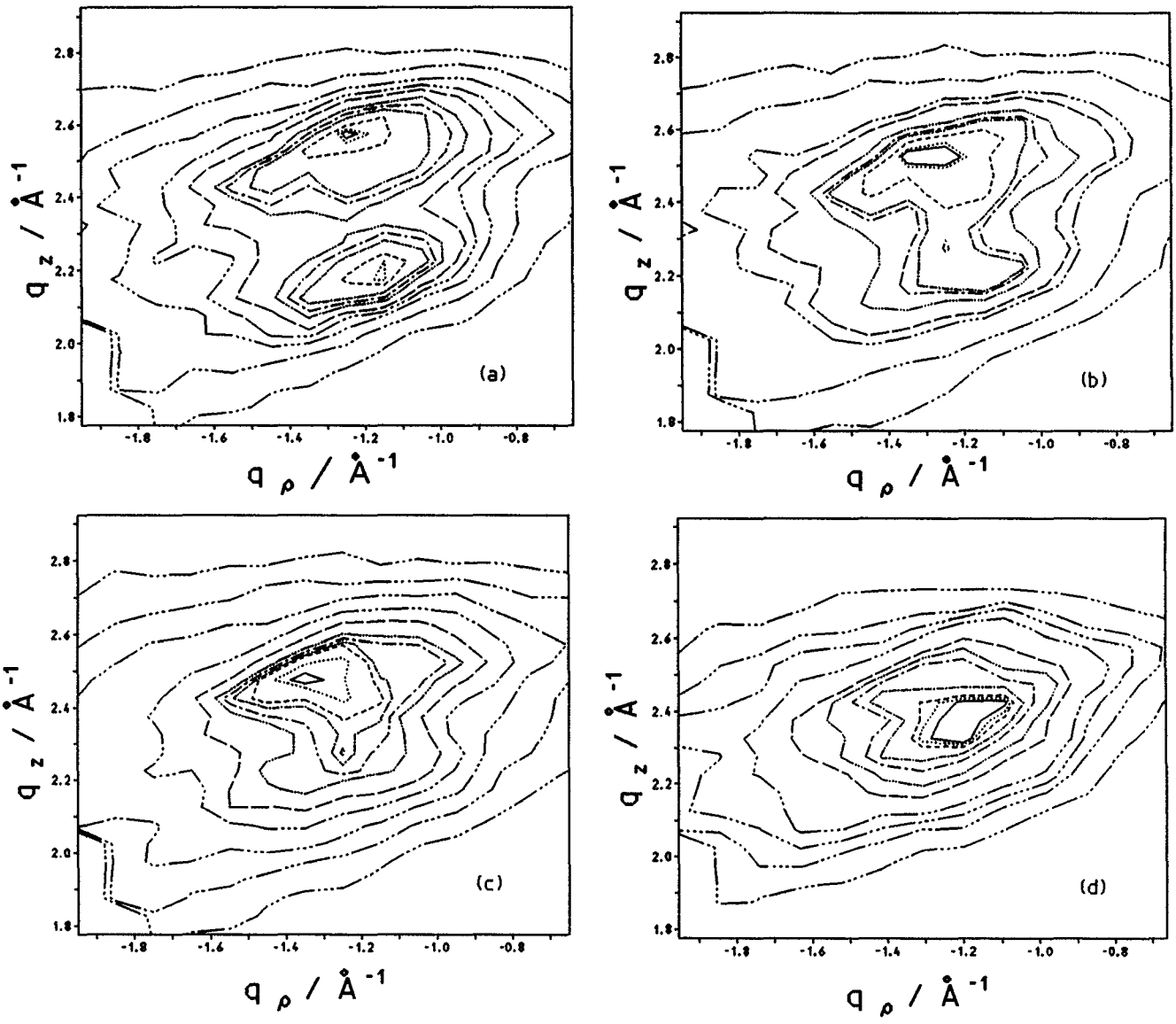

FIG. 6. $C_{20}F_{42}$. Diffuse scattering $S_D(q_\rho,q_z)$ in the range of dominant contributions of first order Bessel functions, measured by neutron scattering at (a) $T=205$; (b) 215; (c) 235; and (d) 275 K within phase R.

$$F_l = F_m(q_\rho,\phi,q_z)$$

$$\approx iJ_1(q_\rho r_f)\exp i\phi\cdot\cos\beta\sum_{l=0}^{19}\exp i(z_l q_z+\varphi_l) - iJ_{-1}(q_\rho r_f)\exp -i\phi\cdot\cos\beta\sum_{l=0}^{19}\exp i(z_l q_z-\varphi_l). \tag{21}$$

The scattering intensity is obtained by a twofold averaging, firstly over ϕ, accounting for the rotation, and second over all molecular conformations

$$\langle F_m F_m^*\rangle = \cos^2\beta J_1^2\sum_{l,l^*=0}^{19}\{\langle\exp i[(z_l-z_l')q_z+(\varphi_l-\varphi_l')]\rangle + \langle\exp i[(z_l-z_l')q_z-(\varphi_l-\varphi_l')]\rangle\}$$

$$= \cos^2\beta J_1^2\sum_{l=0}^{19}(20-l)\{\langle\exp i(\Delta z_l q_z+\Delta\varphi_l)\rangle + \langle\exp i(\Delta z_l q_z-\Delta\varphi_l)\rangle+\mathrm{CC}\}$$

$$= \cos^2\beta J_1^2\sum_{l=0}^{19}(20-l)\{\langle\exp i\chi_l\rangle + \langle\exp i\chi_l'\rangle+\mathrm{CC}\} \tag{22}$$

(CC designates the complex conjugate).

Here Δz_l and $\Delta\varphi_l$ denote the longitudinal and angular displacements between two monomers at a distance l along the chain; χ_l and χ_l' give the phase differences of the scattered waves.

For a perfect helix, χ_l and χ_l' increase linearly with l:

$$\chi_l\sim l,\quad \chi_l'\sim l. \tag{23}$$

Perturbations of the helix by reversal defects in general

result in random fluctuations of χ_l. The values of χ_l become distributed about a certain average value. In general, the width of the distribution will increase together with the distance l. Simple analytical results are obtained if a Gaussian distribution is assumed with a variance

$$\langle \Delta\chi_l^2 \rangle = \langle \Delta\chi_1^2 \rangle \cdot l, \tag{24}$$

and a mean value

$$\langle \chi_l \rangle = (\Delta z q_z - 2\pi t/u) l, \tag{25}$$

which corresponds to the unperturbed helix. This leads to

$$\langle \exp i\chi_l \rangle = \exp - \tfrac{1}{2}\langle \Delta\chi_l^2 \rangle \cdot \exp i\langle \chi_l \rangle$$
$$= \exp - (l/l_c) \cdot \exp il(\Delta z q_z + 2\pi t/u) \tag{26}$$

with

$$l_c = 2/\langle \Delta\chi_1^2 \rangle. \tag{27}$$

The parameter l_c describes a correlation length. For perturbed chains, azimuthal angles are only correlated over a finite number of units in the order of $l \approx l_c$. Equivalently, one obtains

$$\langle \exp i\chi_l' \rangle = \exp - (l/l_c) \cdot \exp il(\Delta z q_z - 2\pi t/u). \tag{28}$$

Insertions of Eqs. (26) and (28) into Eq. (22) yields an expression for $S_D(\mathbf{q})$, which includes l_c as an unknown parameter, together with the basic helix parameters Δz and t/u:

$$S_D(\mathbf{q}) \sim J_1^2 \sum_{l=0}^{19} (20 - l) \exp - l/l_c$$
$$\cdot [\cos l(\Delta z q_z + 2\pi t/u) + \cos l(\Delta z q_z - 2\pi t/u)]. \tag{29}$$

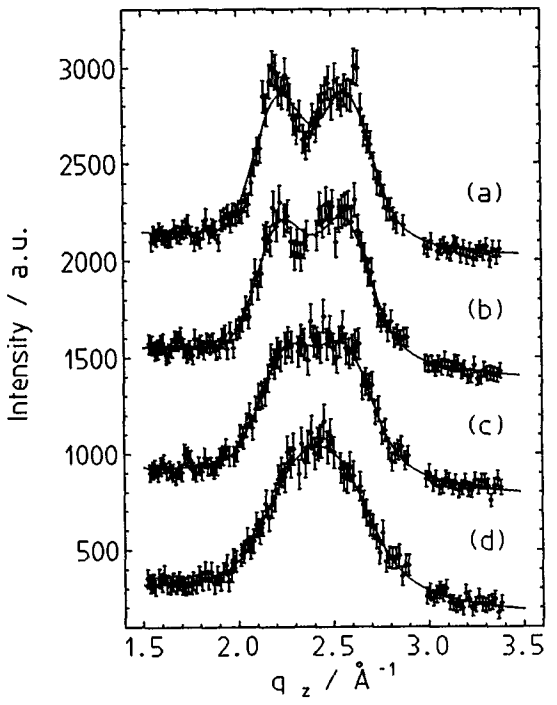

FIG. 7. $C_{20}F_{42}$. Temperature dependence of diffuse scattering $S_D(q_\rho = 1.26\,\text{Å}^{-1}, q_z)$ [(a) 205; (b) 215; (c) 235; (d) 275 K]. Curves are fits on the basis of Eq. (29).

TABLE I. $C_{20}F_{42}$, modification R. Azimuthal correlation length l_c and helix structure parameter u/t are in dependence on temperature.

T (K)	205	215	235	275
l_c	230	168	21	9
u/t	2.155	2.147	2.136	2.10

Comparison with experimental results

Figure 7 demonstrates that Eq. (29) provides an excellent representation of the measured scattering intensities for all temperatures. Curves were determined by conventional fitting procedures, fixing only the value $\Delta z = 1.30$ Å. The parameters l_c and u/t associated with the curves at different temperatures are collected in Table I.

One observes with increasing temperature a decrease in the correlation length l_c, and also a continuous change of the helix structure parameter u/t. A value for l_c much larger than the length of a molecule $l = 20$ indicates that the fraction of molecules, which are perturbed by a helix-reversal defect, is only small. This is the case for $T = 205$ K, i.e., for temperatures near to the phase transition. On the other hand, a correlation length $l_c = 9$ as observed at $T = 275$ K provides evidence for the occurrence of helix-reversal defects in nearly all molecules. We conclude that the helix-reversal defects are formed continuously by thermal activation within phase R.

The change in the helix structure parameter u/t reflects an untwisting process of the helix, which approaches with increasing temperature the all-*trans* form $u/t = 2$. Helix-reversal defects, which include at their center a *trans* conformation, could give support to this process. A direct relation, however, between the defect concentration and the overall conformational state of the helix is not found. The untwisting process begins immediately after the phase transition, which stands in contrast to the formation of helix-reversal defects. The latter become apparent only at more elevated temperatures.

CORRELATED ROTATIONS

If the rotation of the chains in phase R would occur individually without any correlation between neighbors, the molecular scattering, as reflected in the diffuse component S_D, would exhibit cylindrical symmetry

$$S_D \sim \langle |F_m|^2 \rangle (q_\rho, q_z).$$

Measurements give a different result. Evaluation of a Weissenberg photograph obtained for the region of strong diffuse scattering around $q_\rho = 1.3$ Å^{-1}, $q_z = 2.4$ Å^{-1} showed a pronounced variation of S_D with the azimuthal angle. Figure 8(a) presents the intensity distribution $S_D(q_\rho, \phi, q_z = 2.24$ Å$^{-1})$ at 205 K. Six maxima become apparent, located essentially at the positions q_ρ of the strong equatorial reflections. The symmetry of the intensity distribution reflects the symmetry of the rhombohedral Bravais lattice.

Two possible explanations have to be considered.

(i) The azimuthal variation of S_D reflects a nonuniform distribution of the rotational angles of the molecules. Neces-

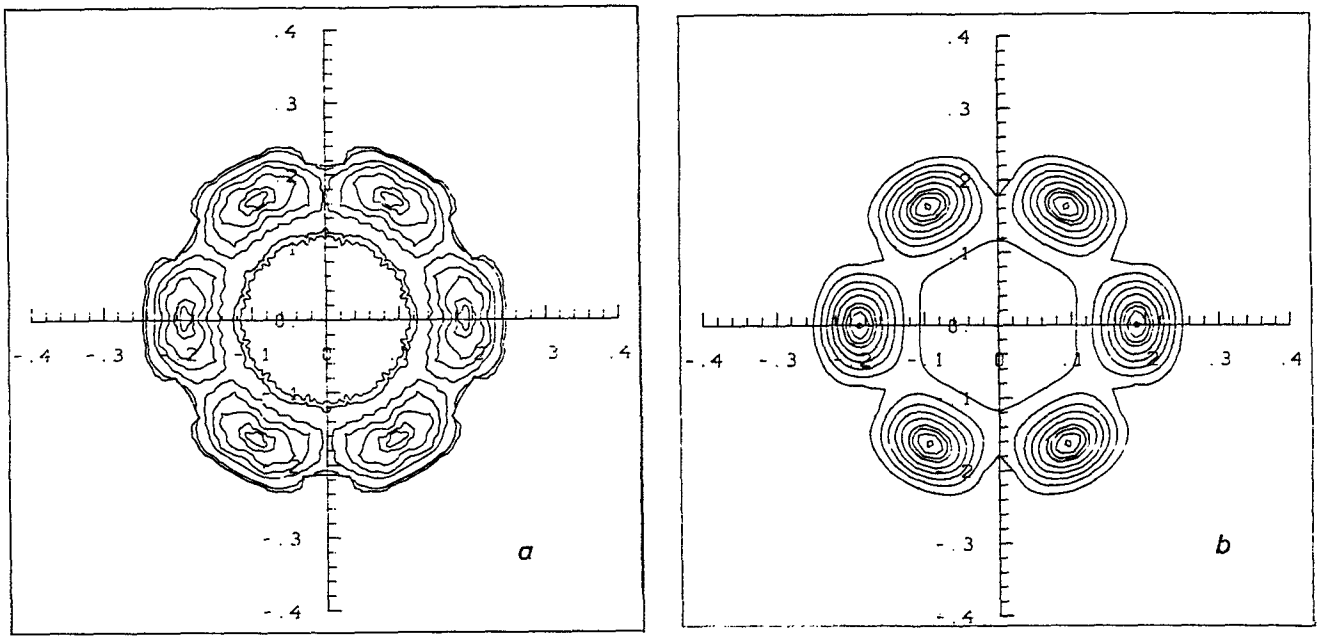

FIG. 8. $C_{20}F_{42}$. $T = 203$ K. (a) Intensity distribution of diffuse scattering $S(q_\rho,\phi,q_z = 2.24\,\text{Å}^{-1})$ obtained for a single crystal by x-ray scattering. (b) Model calculation assuming correlated chain rotations.

sarily, the distribution would then show the symmetry of the lattice.

(ii) The variations of S_D are due to correlations in the chain rotations. Correlations can be accounted for by the introduction of the short-range order function $C(\mathbf{q})$ [Eq. (5)]. This also results in a modification of the intensities which reflects the lattice symmetry.

Case (i) corresponds to a scattering intensity distribution

$$S_D = \int_{\varphi=0}^{2\pi} p(\varphi)\cdot|F_m^\varphi|^2(q_\rho,\phi,q_z)\,d\varphi. \tag{30}$$

F_m^φ denotes the structure factor of a molecule oriented with its short axis (which can be chosen conveniently) in direction φ; $p(\varphi)$ describes the orientational distribution function.

In the range of interest, $|F_m^\varphi|^2(q_\rho,\phi)$ (q_z fixed) is given essentially by the contribution of the first order Bessel function [Eq. (21)] and S_D therefore by

$$S_D(q_\rho,\phi,q_z)\sim J_1^2(q_\rho)\int_\varphi p(\varphi)\sin^2[\phi-\phi_0(\varphi)]\,d\varphi. \tag{31}$$

According to Eq. (31), the shape of the scattering curve in radial direction, i.e., along q_ρ, should be constant and given by $J_1^2(q_\rho)$, independent of ϕ. This is not observed. There is a shift of the maximum between different values of ϕ. Hence, we consider explanation (i) as improbable.

Explanation (ii) is much more convincing. In fact, it enables a good qualitative representation of the scattering data.

Scattering function for correlated chain rotations

Diffuse scattering in the case of correlated fluctuations of the unit cell structure factors is given by Eqs. (5) and (6)

$$S_D(\mathbf{q}) = \langle|\Delta F_i|^2\rangle\cdot C(\mathbf{q}). \tag{5}$$

$$C(\mathbf{q}) = \sum_j \frac{\langle\Delta F_i \Delta F_{i+j}^*\rangle}{\langle|\Delta F_i|^2\rangle}\exp i\mathbf{q}_j\cdot\mathbf{x}. \tag{6}$$

Generally the sum has to be taken over all distance vectors $\mathbf{x}_j$ of the Bravais lattice. We anticipate that in our case, correlation functions $\langle\Delta F_i\Delta F_{i+j}^*\rangle$ give nonnegligible values only for short distances within one layer. The situation around a given molecule is sketched in Fig. 9. There is a first, second, and third shell of six neighbors at distances r_1, r_2, and r_3. We assume equal correlation factors for all six members of one shell. The contribution of the first shell to $C(\mathbf{q})$, which is certainly the most important one, can be directly calculated. It is

$$\sum_{\text{shell }1}\exp i\mathbf{q}\cdot\mathbf{x}_j = \sum_{j=1}^{6}\exp i[q_\rho r_1\cos\delta(\phi,j)], \tag{32}$$

where

$$\delta(\phi,j) = \phi + \frac{\pi}{6} + \frac{\pi}{3}(j-1) \tag{33}$$

denotes the angle enclosed by $\mathbf{q}$ (azimuthal direction ϕ) and the vector pointing to the molecule j. Using a Bessel-function expansion gives

$$\begin{aligned}\sum_{j=1}^{6}\exp i(q_\rho r_1\cos\delta) &= \sum_{j=1}^{6}\sum_{k=-\infty}^{\infty} i^k J_k(q_\rho r_1)\cos[k\delta(\phi,j)] \\ &= \sum_{k=-\infty}^{\infty} i^k J_k \sum_{j=1}^{6}\cos[k\delta(\phi,j)].\end{aligned} \tag{34}$$

The sum over j gives nonvanishing values only for

$$k = 6n \quad (n \text{ integer}).$$

The dominant contributions are given by $k = 0, \pm 6$. Re-

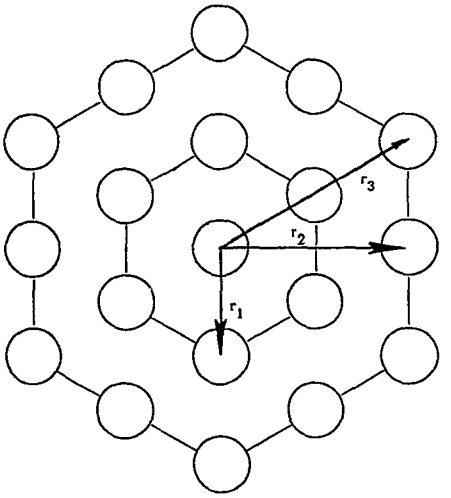

FIG. 9. Shells of neighbors of a given molecule.

stricting the treatment to these three lowest values yields

$$\sum_{j=1}^{6} \exp i\mathbf{q}\cdot\mathbf{x}_j \cong 6[J_0(q_\rho r_1) + 2J_6(q_\rho r_1)\cos 6\phi)]. \quad (35)$$

The sums for the second and third shells can be obtained equivalently, considering that

$$\delta(\phi j) = \phi + \frac{\pi}{3}(j-1)$$

for the second shell, and

$$\delta(\phi j) = \phi + \frac{\pi}{6} + \frac{\pi}{3}(j-1)$$

for the third shell.

The final result is obtained by insertion of Eq. (35) (and the corresponding ones for the second and third shells) into Eq. (6)

$$C(q_\rho,\phi) = 1 + 6C_1[J_0(r_1 q_\rho) + 2J_6(r_1 q_\rho)\cos 6\phi] + 6C_2[J_0(r_2 q_\rho) - 2J_6(r_2 q_\rho)\cos 6\phi] + 6C_3[J_0(r_3 q_\rho) + 2J_6(r_3 q_\rho)\cos 6\phi]. \quad (36)$$

According to Eq. (36),the short-range ordering function $C(\mathbf{q})$ depends only on the correlation coefficients

$$C_j = \frac{\langle \Delta F_i \Delta F^*_{i+j}\rangle}{\langle |\Delta F_i|^2\rangle}. \quad (37)$$

We have performed calculations for different sets of C_j. Figure 8(b) presents the result obtained for

$$C_1 = 0.126, \quad C_2 = 0.028, \quad C_3 = 0.016,$$

which corresponds to an exponential decay of correlations

$$C_j = \exp - r_j/r_c \quad \text{with } r_c = 2.75 \text{ Å}.$$

One arrives at a reasonable qualitative agreement.

Figure 10 shows a simple view for a possible coupling mechanism. The fitting between a right- and a left-handed helix is especially good. It is only retained if rotations are performed for both molecules cooperatively. Hence, a correlated rotation is energetically favored. If the conformation of a molecule is in a mixed state, changing from a right-handed to a left-handed form by the action of helix-reversal defects, and fitting of the surfaces of two adjacent molecules is restricted to shorter sequences, but it may be still effective.

CONCLUSION

Disorder in modification R of perfluoro-*n*-eicosane is set up by different components:

(i) At the transition to phase R, rotation of the chains about their long axes sets in. Rotations occur in a cooperative way, with pronounced correlations between neighbors.

(ii) Interfaces exhibit a moderate roughening originat-

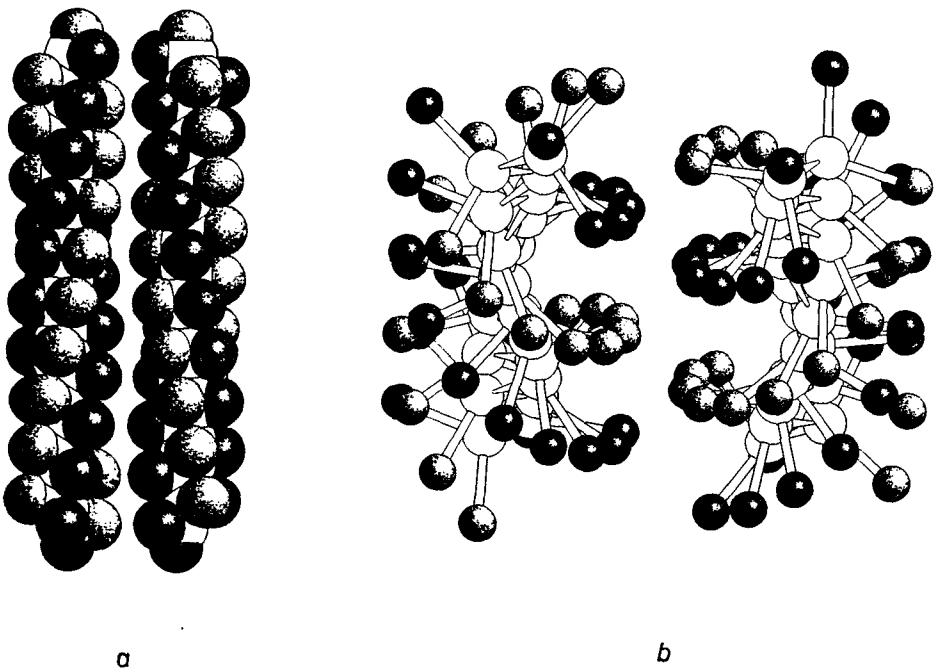

FIG. 10. $C_{20}F_{42}$. (a) A pair of a right- and a left-handed helix. (b) The view under an angle of 5° against the axes, indicating a good fit between ridges and valleys. The favorable contact energy is retained during a cooperative rotation.

ing from longitudinal (or screwlike) motions.

(iii) Molecules are perturbed internally by helix-reversal defects. Defects probably are formed by thermal activation within phase R. Their occurrence leads to an increase in the mean cross section of the molecules.

ACKNOWLEDGMENT

Support of this work by the Ministerium für Forschung und Technologie is gratefully acknowledged.

[1]N. G. Parsonage and L. A. K. Staveley, *Disorder in Crystals* (Clarendon, Oxford, 1978).
[2]*The Plastically Crystalline State*, edited by J. N. Sherwood (Wiley, Clichester, 1979).
[3]H. Schwickert, G. Strobl, and M. Kimmig, J. Chem. Phys. **95**, 2800 (1991).
[4]C. W. Bunn and E. R. Howells, Nature **174**, 549 (1954).
[5]A. Guinier, *X-Ray Diffraction in Crystals, Imperfect Crystals, and Amorphous Bodies*, (Freeman, San Francisco, 1963).
[6]G. Strobl, B. Ewen, E. W. Fischer, and W. P. Piesczek, J. Chem. Phys. **61**, 5259 (1974).
[7]R. G. Brown, J. Chem. Phys. **40**, 2900 (1964).
[8]E. S. Clark, J. Macromol. Sci. Phys. B **1**, 795 (1967).
[9]P. Corradini and G. Guerra, Macromolecules **10**, 1410 (1977).